INT. J. REMOTE SENSING, 1994, VOL. 15, NO. 7, 1447–1458

A two-axis adjusted vegetation index (TWVI)

LI XIA†

Department of Remote Sensing, Guangzhou Institute of Geography, Guangzhou 510070, P.R. China

(Received 12 January 1993; in final form 17 August 1993)

Abstract. Based on the soil line concept, various kinds of vegetation indices have been proposed to minimize soil background influences in the inventory of forest resources and the prediction of vegetation biomass. Unfortunately, those indices can only reduce soil moisture effect on remote sensing data parallel to the axis, the direction of the so-called soil line, failing when different soil types appear (in the direction perpendicular to the soil line). A two-axis adjusted vegetation index is presented here to diminish most soil background influences. It is shown to be more suitable as a global monitoring vegetation index than other indices.

1. Introduction

When remote sensing data are applied to the quantitative study of vegetation status, such as forest canopies and crop production, it is essential to minimize the soil background influences to obtain the pure vegetation information for a mixed pixel. Many approaches have presented vegetation indices with an emphasis on the correction of influences of soil moisture, but those indices cannot represent the true vegetation condition under various soil background. Features of soil background must be understood first for the correction of soil noise. Generally, in the near-infrared (NIR) and red wavelength space, soil spectral plotted points lie approximately along a line called the soil line with a slope close to 1 and a near-infrared NIR intercept close to 0. If the soil background becomes wet, a vegetated pixel will move towards the origin of the spectral space parallel to the soil line.

Many spectral vegetation indices, (see Tucker 1979), have been developed to reduce soil background influences. The earliest study involved the infrared/red ratio by Colwell (1973, 1974) which concluded that the NIR/red ratio was effective in minimizing the effect of soil background variation. Rouse *et al.* (1973, 1974) (see Tucker 1979) reported that although a simple ratio of Landsat MSS bands (MSS7/MSS5) could be applied as an indication of greenness, location and cycle deviation would produce a large error component. The difference between the MSS7–MSS5 radiance values, normalized over the sum of MSS7+MSS5, was used as an index value (NDVI). The constant of 0·5 was added and a square-root transformation was applied to avoid a negative value (TVI). Kauth and Thomas (1976) (see Tucker 1979) developed a technique to transform Landsat multi-dimension data into a soil brightness index (SBI) and a green vegetation index (GVI) using all the bands. Jackson (1983), and Huete *et al.* (1984) also presented spectral indices in the *n*-space.

†Present address (before the end of 1995): The Centre of Urban Planning and Environmental Management, The University of Hong Kong, Pokfulam Road, Hong Kong.

0143–1161/94 $10.00

Richardson and Wiegand (1977) proposed a departure from the soil background line with the perpendicular vegetation index (PVI). Huete (1988) presented a transformation technique to normalize soil brightness influences by a vegetation index involving near-infrared (NIR) and red wavelengths. The transformation graphically shifts the origin of reflectance spectra plotted in the NIR-red wavelength space to account for first axis soil-vegetation behaviour and the differential NIR and red flux extinction through vegetated canopies, presenting a concise SAVI model (soil-adjusted vegetation index) based on NDVI.

The various vegetation indices with emphasis on obtaining pure vegetation information under the context of the mixed pixel may include:

1. Ratio index (RVI)
   $RVI = NIR/red$
   Where NIR and red are reflectance in near-infrared and red wavelength.
2. Differential vegetation index
   $NIR - \text{red}$
3. Normalized difference vegetation index ($NDVI$)
   $NDVI = (NIR - red)/(NIR + red)$
4. Transformed vegetated index (TVI)
   $TVI = \sqrt{NDVI + 0{\cdot}5}$
5. Kauth and Thomas's green vegetation index (GVI)
   $GVI = -0{\cdot}29\text{MSS4} - 0{\cdot}56\text{MSS5} + 0{\cdot}60\text{MSS6} + 0{\cdot}49\text{MSS7}$
6. Perpendicular vegetation index (PVI)
   $PVI = \sqrt{(Red_{soil} - Red_{veg})^2 + (NIR_{soil} - NIR_{veg})^2}$
7. Soil-adjusted vegetation index ($SAVI$)
   $SAVI = ((NIR - red)/(NIR + red + L))(1 + L)$

Where L is a constant which is chosen by experiment.

However although these vegetation indices are very useful in minimizing the soil background influences in the direction of the first axis, they can do nothing in the secondary axis of soil background.

Having recognized the complexity of soil variation, Jasinsky and Eagleson (1989) presented the concept of hypothetical soil lines in the study of semi-vegetated landscapes (figure 1). Those soil lines are more close to the real situation of soil background than the conventional single soil line.

Real soil scenes contain a composite of several types of variability. Thus, variability of any one soil parameter can lead to a representative line in a two-dimensional scattergram. Actually, those soil lines can be projected on two axes and decomposited into two components. The first is in the direction of the soil moisture line which is usually considered as the soil line. The second is vertical to the soil line that consists of all variations of soil background other than soil moisture. In this paper, a two-axis adjusted vegetation index (TWVI) is presented for the global correction of the influence of soil variation.

2. Approach

2.1. *Spectral characteristics of soil background*

In the NIR-red wavelength space, the plotted points of soil spectra are aggregated within an elliptical area. Producing a scattergram of non-vegetated soil pixel for satellite data is a simple way to analyse the characteristics of soil background.

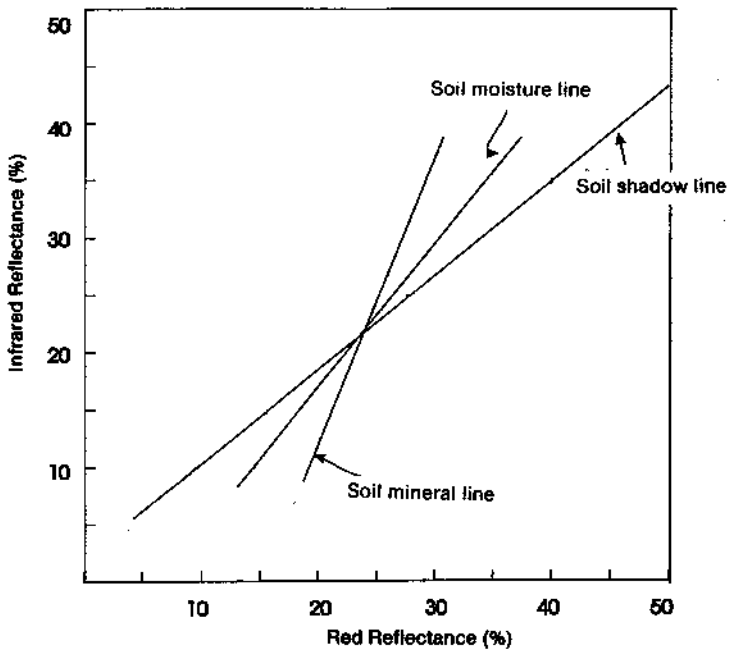

Figure 1. The complexity of soil background (Jasinsky and Eagleson 1989).

Statistic analysis shows the scattergram belongs to a normal distribution that can be represented by a ellipse in a two-dimension space.

Non-vegetated soil pixel data of Landsat TM bands 3 and 4 (TM3 and TM4) (TM CCT of Guangzhou, P.R. China, 10 December, 1988) were analysed using ARIES-II image processing software. These pixels are confined within an elliptical area after being plotted in the NIR-red wavelength space (figure 2). Statistical analysis reveals that those remote sensing data are of normal distribution. The location, direction and shape of the ellipse are identified by the two features, mean vector and variance matrix.

Mean vector:

$$\begin{pmatrix}\overline{TM_4}\\ \overline{TM_3}\end{pmatrix}=\begin{pmatrix}30{\cdot}98\\ 29{\cdot}10\end{pmatrix}$$

Variance matrix:

$$\sum_x=\begin{pmatrix}24{\cdot}373 & 17{\cdot}151\\ 17{\cdot}151 & 17{\cdot}390\end{pmatrix}$$

The direction and length of the two axes of the ellipse can be derived from the variance matrix. The first axis (long axis) which represents the conventional soil line reflects the soil wetness, and the secondary axis (short axis), includes the information of the chromas of the soil (red or yellow coloured soils) (see Huete 1988).

Thus, the equation of soil line (long axis) is calculated;

$$TM_4=0{\cdot}816TM_3+7{\cdot}234$$

The direction vector of the soil line is: (0.816,1)

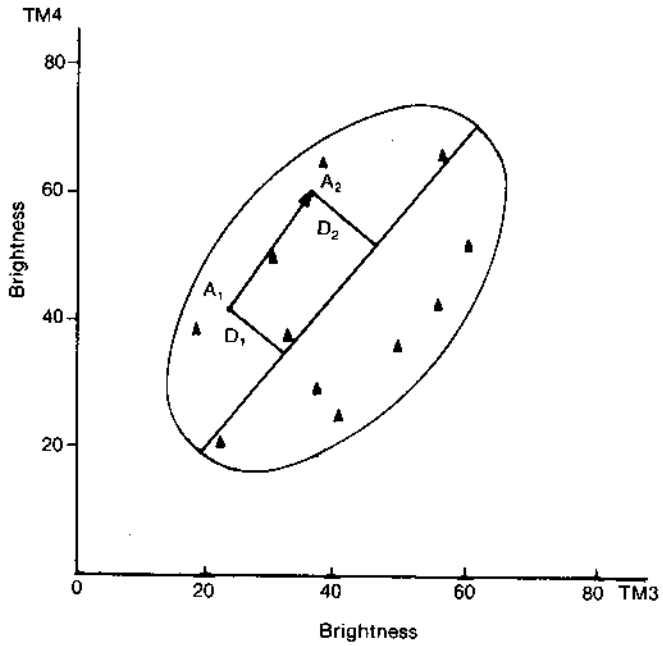

Figure 2. The position change from A_1 to A_2 for a same pixel of soil background on 10 December 1988 and 13 October 1990; Guanghou P.R., China).

The soil variation in the two direction can be relatively represented by the lengths of the two axes:

$$\frac{\text{The length of short axis}}{\text{The length of long axis}}=\frac{\sqrt{\lambda_2}}{\sqrt{\lambda_1}}=\frac{0{\cdot}162}{0{\cdot}544}=0{\cdot}298$$

where λ_1 and λ_2 are the two feature values of the variance matrix.

Since the length of secondary axis is $1/2 \sim 1/4$ of the length of the first axis (the soil line) of the soil ellipse, the variation in the secondary axis cannot be ignored in order to derive a vegetation index.

Here the distance D of a non-vegetated pixel (TM_4, TM_3) from the first axis (soil line) is used to account for the variation in the secondary axis.

Suppose equation of the soil line is:

$$A\,TM_4+B\,TM_3+C=0 \tag{1}$$

A vegetated pixel deviates away from its theoretical location that meets the ideal condition of one-axis adjusted indices in the direction perpendicular to the soil line under the soil variation in the secondary axis. The deviation is contributed by the distance offset D.

$$D=\frac{A\,TM_4+B\,TM_3+c}{\sqrt{A^2+B^2}} \tag{2}$$

The error produced by the soil variation in the secondary axis can be corrected from the distance offset D. A vegetated pixel can be adjusted to its original location with pure vegetation information.

Table 1. Distance offset D_1 and D_2 of non-vegetated soil background on two dates.

	10 December 1988			13 October 1990		
Site	TM_4	TM_3	D_1	TM_4	TM_3	D_2
1	34	23	6·2	43	26	7·8
2	29	36	−5·3	25	29	−5·7
3	31	23	3·8	31	23	2·7
4	18	22	−5·6	29	32	−5·6
5	40	43	1·8	42	40	3·2
6	37	18	11·7	45	22	12·2
7	39	31	5·0	46	30	6·5
8	20	26	−6·5	28	30	−4·6
9	20	27	−7·2	32	34	−5·3
10	19	23	−5·4	36	39	−6·7
11	31	36	−4·3	41	41	−5·2
12	39	25	12·2	45	22	8·8

Non-vegetated data of remote sensing from different periods are applied to reveal the seasonal spectral changes of distance offset D. The following table gives the distance offset D_1 and D_2 of some non-vegetated soil pixels on two dates (10 December, 1988 and 13 October, 1990, Guangzhou, P.R. China).

There are not too many seasonal spectral changes in the secondary axis for the same non-vegetated pixel (figure 2). The obvious change only takes place in the direction of the first axis, which contributes to the variation of soil moisture. Since D does not change too much on different dates for a same non-vegetated pixel it can be derived conveniently from remote sensing data or field measurement in an appropriate time.

2.2. *A two-axis adjusted vegetation index (TWVI)*

Let us consider the situation of a surface, partly covered with green vegetation and partly bare. The total measured reflectance R will then be equal to (Suits 1972, Clevers 1988):

$$R = R_\infty(1 - e^{-KLAI}) + R_S e^{-KLAI} \tag{3}$$

Where R is the total measured reflectance, R_∞ is the reflectance of the vegetation (complete cover), R_S is the reflectance of the soil, K is the extinction coefficient, and LAI is leaf area index. R can be obtained from remote sensing data, and R_∞ and R_S can be measured by field work. Thus, LAI can be derived from the formula. However, it is impractical to measure R_S since R_S varies from place to place.

Ratio or difference transformation have been applied to reduce the soil influence on remote sensing data. The soil line is used usually to depict the spectra features of soil background.

$$NIR_S = M\, red_S + I \tag{4}$$

Where NIR_S is the reflectance of the soil background in the near-infrared wavelength, red_S is the reflectance of the soil background in red wavelength, and M is the slope of the soil line equation.

Equation (3) can be expressed in terms of the NIR and red wavelength as:

$$NIR = NIR_{\infty}(1 - e^{-KLAI}) + NIR_S e^{-KLAI} \tag{5}$$

$$red = red_{\infty}(1 - e^{-KLAI}) + red_S e^{-KLAI} \tag{6}$$

where NIR_{∞} and red_{∞} are reflectance of complete cover in NIR and red wavelength.

(The difference in red and NIR canopy extinction is ignored here.)

When $I = 0$, (since the NIR intercept is close to 0), then (4), (5) and (6) can be solved to obtain:

$$LAI = -\frac{1}{K}\ln(1 - PI/((NIR_{\infty} - M\,red_{\infty})\cos\theta)) \tag{7}$$

where $\cos\theta = 1/\sqrt{1+M^2}$, $\sin\theta = M/\sqrt{1+M^2}$, and $PI = NIR\cos\theta - red\sin\theta$.

After calculating PI using remote sensing data, we can compute isolines of LAI as a series of lines parallel to the soil line.

Actually, canopy extinction K has different values for the NIR and red wavelength. K_{red} is always greater than K_{NIR} for a photosynthetically active canopy (Huete 1988). These are:

$$NIR = NIR_{\infty}(1 - e^{-K_{NIR}LAI}) + NIR_S e^{-K_{NIR}LAI} \tag{8}$$

$$red = red_{\infty}(1 - e^{-K_{red}LAI}) + red_s e^{-K_{red}LAI} \tag{9}$$

Equations (4), (8) and (9) are solved to derive:

$$NIR = M e^{(K_{red} - K_{NIR})LAI} red + (1 - e^{-K_{NIR}LAI})NIR_{\infty} - M e^{(K_{red} - K_{NIR})LAI}(1 - e^{-K_{red}LAI})red_{\infty} + I e^{-K_{NIR}LAI} \tag{10}$$

The slope of a LAI isoline is

$$M_{LAI} = M\exp(K_{red} - K_{NIR})LAI \tag{11}$$

where M_{LAI} is the slope of a LAI isoline.

Equation (11) reveals that the slope of a LAI isoline is dependent on the slope M of the soil line, the leaf area index LAI, and the K is difference in NIR and red wavelength. When the $K_{red} = K_{NIR}$, the slope of the isolines remains constant and equal to the slope of the soil line. Huete *et al.* (1985, 1988) has proved that $K_{red} > K_{NIR}$ (a photosynthetically active canopy). Both Huete's field data and ours have showed that the slope of the isolines becomes greater with the increment of the LAI value. Huete discovered that the real vegetation isolines possesses NIR-red wavelength slopes in between those of the ratio (RVI, $NDVI$) and orthogonal-based (PVI) isolines. In Huete's study, soil-vegetation spectral behaviour is modelled graphically through adjustment of the $NIR - red$ wavelength space origin to various isoline convergence. A soil adjusted vegetation index ($SAVI$) was given to involve an addition of a constant, L, to the denominator of the NDVI equation (see figure 3).

$$SAVI = ((NIR + l_2) - (red + l_1))/((NIR + 1_2) + (red + l_1)) \tag{12}$$

Since the soil line has a slope close to 1, the adjustment factors, l_1, and l_2 would be nearly equivalent

$$SAVI = (NIR - red)/(NIR + red + L) \tag{13}$$

where $L = l_1 + l_2$.

A multiplication factor $(1+L)$ is needed

$$SAVI=((NIR-red)/(NIR+red+L))(1+L) \tag{14}$$

Although there are various L values, a single optimal L value can be applied to a wide range of vegetation deneities, depending on where one wishes to analyse very low vegetation densities ($L=1$), intermediate densities ($L=0{\cdot}5$), or higher densities ($L=0{\cdot}25$). An adjustment factor for intermediate vegetation amounts ($L=0{\cdot}5$) can offer a spectral index superior to the NDVI and PVI for the entire range of vegetation conditions. The SAVI can substantially reduce soil-produced variations and improve the linearity between index and LAI in comparison to the NDVI and PVI.

However, neither the PVI and RVI (NDVI), nor the SAVI remove the disturbance introduced by soil background in the secondary axis. They succeed in correcting soil brightness (wet soil and dry soil) influences, but fail when soil types are of great variations (solid material changes). Huete also admitted that although SAVI is superior to NDVI and PVI, it will not compress this secondary source of soil variations, (red soil and yellow soil), as only the soil line orientation problems and soil brightness effects on vegetation isolines are modelled.

Thus, the two-axis adjusted vegetation index TWVI is proposed based on the SAVI model. Since plotted points of the non-vegetated soil spectra are confined within an elliptical area and a soil line does not really exist, a general soil line is defined here:

$$NIR_S=M\,red_S+I+D \tag{15}$$

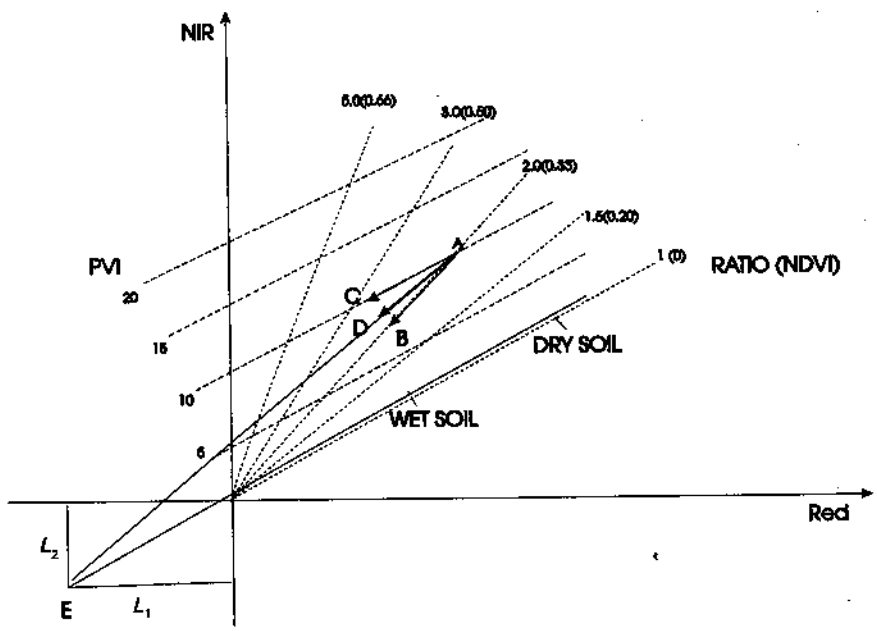

Figure 3. The *SAVI* model and its relation with *RVI* (*NDVI*) and *PVI* (Huete 1988).

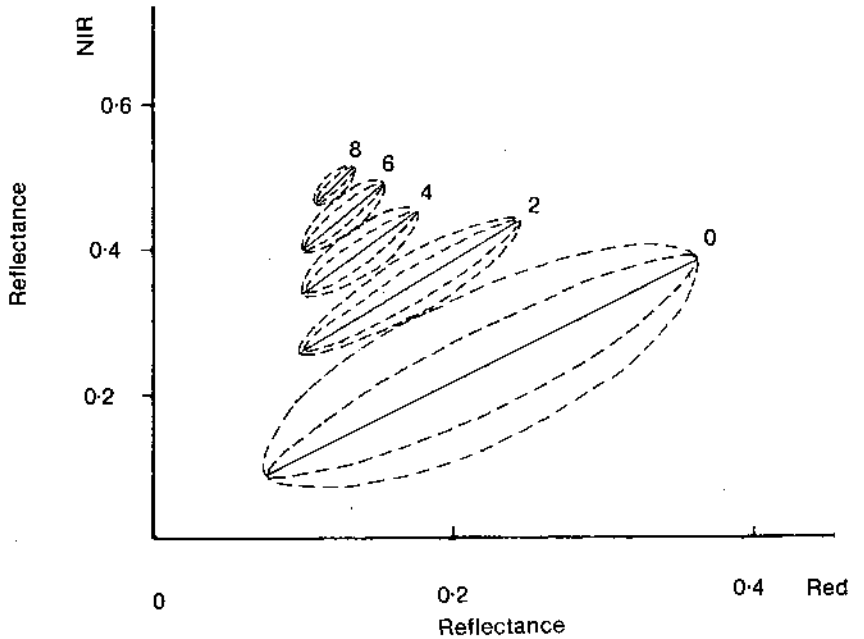

Figure 4. *LAI* isolines in the *TWVI* model.

Table 2. Measured reflectance of various *LAI* value under different soil background.

Value / Soil	*LAI*=0		*LAI*=2		*LAI*=4		*LAI*=6		*LAI*=8	
	TM_3	TM_4	TM_3	TM_4	TM_3	TM_4	TM_3	TM_4	TM_3	TM_4
1. Organic	0·09	0·15	0·10	0·24	0·10	0·34	0·11	0·40	0·11	0·47
2. Sandy	0·31	0·38	0·25	0·41	0·17	0·44	0·16	0·47	0·14	0·51

Table 3. Index values for various *LAI* under the soil background.

Index / *LAI*	*RVI*		*NDVI*		*PVI*		*SAVI*		*TWVI*	
	1	2	1	2	1	2	1	2	1	2
2	2·40	1·64	0·41	0·24	0·11	0·09	0·25	0·21	0·22	0·22
4	3·40	2·59	0·55	0·44	0·21	0·22	0·38	0·36	0·36	0·37
6	3·64	2·94	0·57	0·49	0·25	0·26	0·43	0·41	0·42	0·42
8	4·27	3·64	0·62	0·57	0·32	0·33	0·50	0·48	0·49	0·49
error %	27·6		26·8		5·2		5·8		0·7	

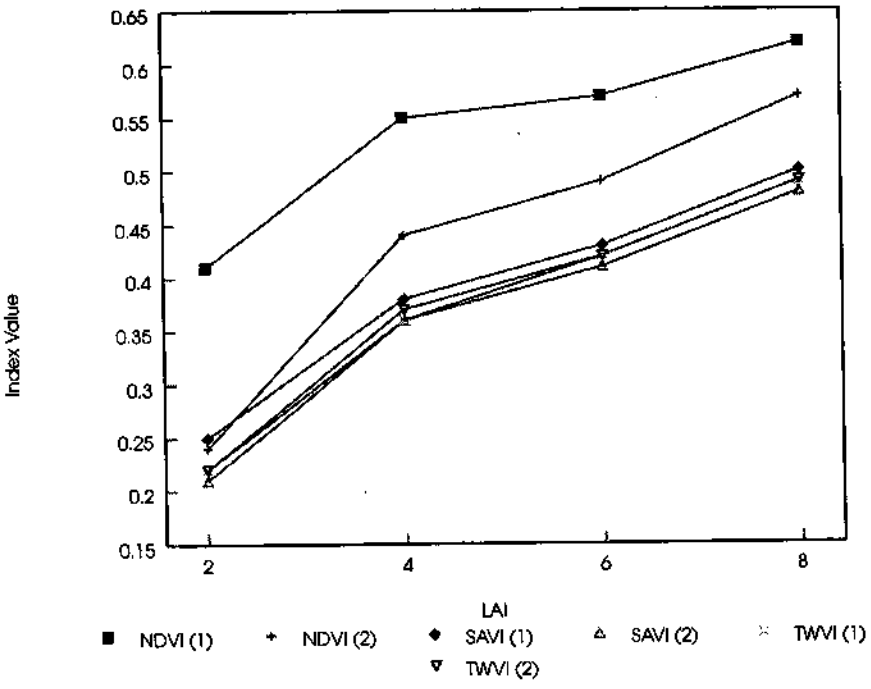

Figure 5. Vegetation Index Response of the NDVI, SAVI, TWVI under Two Soil Types (1: organic soil; 2: sandy soil).

Where D is the distance offset from a non-vegetated soil pixel (NIR_S, red_S) to the conventional soil line.

$$D=(NIR_S-M\,red_S-1)/(\sqrt{1+M^2}) \tag{16}$$

After solving equations of (15), (8) and (9), we have:

$$NIR=M\,e^{(K_{red}-K_{NIR})LAI}red+(1-e^{-K_{NIR}LAI})NIR_\infty-M\,e^{(K_{red}-K_{NIR})LAI}\times(1-e^{-K_{red}LAI})red_\infty+(I+D)e^{-K_{NIR}LAI} \tag{17}$$

Although LAI can be deduced from remote sensing data (NIR, red) by the formula after the parameters of I, D, K_{red}, K_{NIR}, red_∞ and NIR_∞ are measured, a simple model $TWVI$ based on $SAVI$ is given here to replace the complicated solution.

When a physical single soil line (conventional) existed, namely, all non-vegetated soil pixels fell on a line ($D=0$), Huete (1988) presented a graphical transformation ($SAVI$). Based on NDVI, the algorithm involves a shifting of the origin of the reflectance spectra plotted in the NIR-red wavelength space to account for first-order soil-vegetation interactions and differential red and NIR flux extinction through vegetated canopies.

The remote sensing data (NIR, red) for a given pixel in the two-dimension space consists of the information of two components: vegetation and soil background. If a single soil line existed, $SAVI$ would be a good solution to obtain pure vegetation information. Actually, in most situations, the soil plotted points in spectral space

deviate away from the soil line, and the second axis ($D=0$) can create an error if an adjustment in the direction is ignored. The original data (*NIR*, *red*) can be corrected to a new position (*NIR'*, *red'*) after removing an increment (*dNIR*, *dred*) produced by *D* from (*NIR*, *red*). So far, the new position (*NIR'*, red') can get rid of the secondary variation.

$$NIR' = NIR - dNIR \tag{17}$$

$$red' = red - dred \tag{18}$$

(The *K* difference in *NIR* and the *red* canopy extinction can be ignored here because *SAVI* itself has taken it into account.)

After differentiating (5) and (6), we obtain

$$dNIR = e^{-KLAI}\, dNIR_S \tag{19}$$

$$dred = e^{-KLAI}\, dred_S \tag{20}$$

$dNIR_S$ and $dred_S$ are the projecton of the soil offset *D* in the *NIR* axis and *red* axis. They result in the deviation of remote sensing data (*NIR*, *red*) that will produce an error for a one-axis vegetation index.

$$dNIR_S = D\cos_\theta \tag{21}$$

$$dred_S = -D\sin_\theta \tag{22}$$

Where $\cos\theta = 1/\sqrt{1+M^2}$ and $\sin\theta = M/\sqrt{1+M^2}$.

Equations (19) and (20) suggest that the deviation of (*NIR*, *red*) come from the distance offset *D*. The influence of soil background decreases in an exponential function when *LAI* increases. Soil variation in the secondary axis has an impact on the vegetation index and cannot be ignored when the vegetation is not a complete cover.

Since the slope of the ordinary soil line is close to 1, there are:

$$dNIR_S = -dred_S = \frac{\sqrt{2}}{2} D \tag{23}$$

$$dNIR = -dred = \frac{\sqrt{2}}{2} e^{-KLAI} D \tag{24}$$

Equations of (4), (5) and (6) are solved to get:

$$\begin{aligned} e^{-KLAI} &= 1 - (NIR - M\,red - I)/(NIR_\infty - M\,red_\infty - I) \\ &= 1 - (I_\lambda - I)/(I_\infty - I) \end{aligned} \tag{25}$$

Where $(I_\lambda - I)/(I_\infty - I) = (NIR - M\,red - I)/(NIR_\infty - M\,red_\infty - I)$.

$(I_\lambda - I)/(I_\infty - I)$ can indicate the distance between the pixel (*NIR*, *red*) and the complete cover pixel (NIR_∞, red_∞) in the spectral space. When the point (*NIR*, *red*) is on the soil line (non-vegetation), $(I_\lambda - I)/(I_\infty - I) = 0$; when point (*NIR*, *red*) is equal to (NIR_∞, red_∞) (complete cover), $(I_\lambda - I)/(I_\infty - I) = 1$.

The two-axis adjusted model based on *SAVI* is deduced after the adjustment of (*NIR*, *red*) by distance offset *D*.

$$TWVI=(((NIR-dNIR)-(red-dred))/((NIR-dNIR)+(red-dred)+L)))(1+L) \quad (26)$$

dNIR, *dred* are replaced by using (24) and (25):

$$TWVI=((NIR-red-\Delta)/(NIR+red+L))(1+L) \quad (27)$$

Where $\Delta=\sqrt{2}\,e^{-KLAI}D=\sqrt{2}\,(1-(I_\lambda-I)/(I_\infty-I))\,D$

Δ is the deviation of the remote sensing data (*NIR*, *red*) caused by the soil distance offset D in the secondary axis. When $D=0$ ($\Delta=0$), *TWVI* becomes *SAVI* (influences of soil variation in secondary axis is ignored); when $\Delta=0$ and $L=0$, *TWVI* becomes *NDVI* (influences of soil variation in secondary axis and the difference in *NIR* and red canopy extinction are not taken into account.

That vegetation isolines in the *TWVI* model are uncertain (figure 4) is contrary to the fact that there is a unique isoline for an LAI value in those models (*RVI*, *NDVI*, *PVI* and *SAVI*). For each pixel, (*NIR*, *red*) has not a unique *TWVI* value because of the deviation caused by the soil background. The LAI isolines in the *TWVI* model are strongly influenced by soil ellipse (figure 4). There is more than one isoline for a given LAI value under the influence of the secondary axis. Other conventional models (*RVI*, *NDVI*, *PVI*, and *SAVI*) use a unique LAI isoline corresponding to a specific LAI value.

3. Discussion

Field study was carried out to compare *TWVI* with those conventional indices, using spectral data over a series of grass canopies on different soil background. The HHRR spectrometer with seven bands corresponding to the TM bands was used to obtain spectral data for the different LAI value under two types of soil background in local time, 9.30–10.30 a.m.

This experiment was carried out by alternating a series of grass canopies on two soil types which were both of solid material variation and moisture difference. The soil types were: (1) organic soil; (2) sandy soil. The distinctions could introduce spectral deviations in both the first axis (caused by soil moisture condition) and the secondary axis (caused by solid material variation).

The equation of soil line was obtained from measured data:

$$TM_4=1{\cdot}23\,TM_3+0{\cdot}01 \quad (28)$$

The distance offset of the two soil types in secondary axis was calculated by (16):

$$D'=0{\cdot}018 \quad \text{and} \quad D''-0{\cdot}007.$$

Spectral data were measured by putting grass of different LAI on the two soil background. Calculated results of the measurement can indicate which index is superior in minimizing the soil impact (Tables 2 and 3).

A good vegetation index should have the ability to deduce a unique value for the same vegetation condition no matter how the soil background changes. There are obvious errors in the *RVI*, *NDVI*, *PVI* and *SAVI* models (see figure 5) in this experiment because they exclude the secondary axis correction. Although the difference of distance offset D is not too great, *TWVI* has improved the precision by 26 per cent higher than those of RVI and NDVI, 5 per cent higher than those of *PVI* and *SAVI*. When D is great, *TWVI* is believed to have more advantages than those

indices. It has potential as a global index to monitor the dynamic soil-vegetation systems.

References

COLWELL, J. E., 1973, Bidirectional spectral reflectance of grass canopies for determination of above ground standing biomass, Ph.D. thesis, University of Michigan, University Microfilm 75-15, 693.

COLWELL, J. E., 1974, Vegetation canopy reflectance. *Remote Sensing of Environment*, **3**, 175-183.

CLEVERS, J. G. P. W., 1988, The derivation of a simplified reflectance model for the estimation of leaf area index. *Remote Sensing of Environment*, **25**, 53-69.

HUETE, A. R., POST, D. F., and JACKSON, R. D., 1984, Soil spectral effects on 4-space vegetation discrimination, *Remote Sensing*, **15**, 155-165.

HUETE, A. R., JACKSON, R. D., and POST, D. F., 1985, Spectral response of a plant canopy with different soil backgrounds. *Remote Sensing of Environment*, **17**, 37-53.

HUETE, A. P., 1988, A soil-adjusted vegetation index (SAVI), *Remote Sensing of Environment*, **25**, 295-309.

JACKSON, R. D., 1983, Spectral indices in *n*-space. *Remote Sensing of Environment*, **13**, 409-421.

JASINSKI, M. F., and EAGLESON, P. S., 1989, The structure of red-infrared scattergrams of semivegetated landscapes. *I.E.E.E. Transactions on Geoscience and Remote Sensing*, **27**, 441-451.

RICHARDSON, A. J., and WIEGAND, C. L., 1977, Distinguishing vegetation from soil background information. *Photogrammetric Engineering and Remote Sensing* (Falls Church, VA: American Society for Photogrammetry and Remote Sensing), **43**, 1541-1552.

SUITS, G. H., 1972, The calculation of the directional reflectance of a vegetative canopy. *Remote Sensing of Environment*, **2**, 117-125.

TUCKER, C. J., 1979, Red and photographic infrared linear combination for monitoring vegetation. *Remote Sensing of Environment*, **8**, 127-150.